

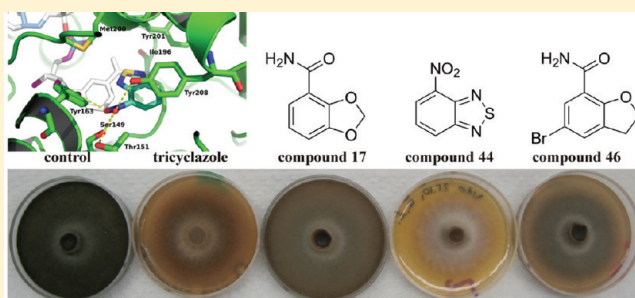
Novel Inhibitors of Trihydroxynaphthalene Reductase with Antifungal Activity Identified by Ligand-Based and Structure-Based Virtual Screening

Mojca Brunskole Švegelj,[†] Samo Turk,[‡] Boris Brus,[‡] Tea Lanišnik Rižner,[†] Jure Stojan,[†] and Stanislav Gobec^{*,†}

[†]Institute of Biochemistry, Faculty of Medicine, University of Ljubljana, Vrazov trg 2, 1000 Ljubljana, Slovenia

[‡]Faculty of Pharmacy, University of Ljubljana, Aškerčeva 7, 1000 Ljubljana, Slovenia

ABSTRACT: *Curvularia lunata* is a dark pigmented fungus that is the causative agent of several diseases in plants and in both immunodeficient and immunocompetent patients. 1,8-Dihydroxynaphthalene-melanin is found in the cell wall of *C. lunata* and is believed to be the important virulence factor of dematiaceous fungi. Trihydroxynaphthalene reductase is an enzyme of the 1,8-dihydroxynaphthalene-melanin biosynthetic pathway, and it thus represents an emerging target for the development of novel fungicides and antimycotics. In the present study, we describe novel inhibitors of trihydroxynaphthalene reductase from *C. lunata*. These inhibitors were identified by ligand-based three-dimensional similarity searching and docking to a homology-built model and by subsequent biochemical and antifungal evaluation. Discovery of competitive inhibitors with K_i values in low micromolar and even nanomolar concentration range proves the applicability of homology-built model of 3HNR for hit finding by virtual screening methods.



INTRODUCTION

Curvularia lunata is a dark pigmented saprobic mold that is found primarily in soil.¹ It is a known plant and human pathogen. The plant diseases include leaf blight on *Sorghum*, leaf spot on *Cannabis sativa*, seedling blight on *Saccharum* spp, and stem necrotic lesions on *Hylocereus polyrhizus*.^{2,3} By reviewing the published literature, we also found several case reports of *C. lunata* as the causative agent of diseases in both immunocompromised and immunocompetent individuals. Clinical manifestations of *C. lunata* infections include allergic fungal sinusitis, endocarditis, peritonitis, eumycetoma, keratitis, allergic bronchopulmonary disease, endophthalmitis, optic neuropathy, and disseminated phaeohyphomycosis.^{1,4–14} The number of case reports on disseminated phaeohyphomycosis has increased in recent years, mostly, although not exclusively, in patients with iatrogenic immunodeficiency. There are limited therapeutic options for the treatment of these frequently fatal infections (overall mortality rate, 79%), and thus new antifungal agents and therapeutic options are urgently needed.¹³

Dematiaceous, or dark pigmented fungi, contain melanins in their cell walls that protect them against environmental stress and enable their survival under extreme conditions.^{15,16} In addition, melanization is associated with fungal virulence and pathogenicity, and it reduces fungal susceptibility to host defense mechanisms and enables plant pathogenic species to enter into plant tissue.^{15–17} The wide variety of plant and/or human pathogenic dematiaceous fungi synthesize their melanins from 1,8-dihydroxynaphthalene (DHN)-melanin via the pentaketide pathway.^{15,18}

As the synthesis of DHN-melanin does not occur in host organisms, enzymes participating in this biosynthetic pathway represent emerging targets for the development of selective fungicides and antimycotics. One of the enzymes involved in DHN-melanin biosynthesis is trihydroxynaphthalene reductase (3HNR), which reduces 1,3,8-trihydroxynaphthalene to vermeline.¹⁹ Recently, we cloned, overexpressed, and purified 3HNR from *C. lunata* and identified its first inhibitors by biochemical screening.^{20–22}

To date, only a few inhibitors of 3HNR are known. Among these, there are the commercially available agents of tricyclazole, pyroquilon, and phthalide,²³ some nonsteroidal anti-inflammatory drugs, 1,3-indandione, and compounds with a chromen-4-one scaffold,²⁰ plus several natural compounds, like flavones, flavonols, isoflavones, and flavanones.²² The crystal structure of 3HNR from *C. lunata* is not solved; however, a homology-built model is available.²⁰ In the present study, we report on our successful use of both ligand-based three-dimensional (3D) similarity searching and docking to this homology-built model to define novel potent inhibitors of 3HNR from *C. lunata* that show antifungal activity.

MATERIALS AND METHODS

Computer Hardware. All of the computational procedures were carried out on two workstations. The first workstation has

Received: March 29, 2011

Published: June 13, 2011

four dual core AMD Opteron 2.0 GHz processors, 16 GB RAM, four 320 GB hard drives in a RAID10 array, and Nvidia GeForce 7900 graphic cards; this workstation is running the 64-bit fedora 7. The second workstation has two quad core Intel Xeon 2.2 GHz processors, 8 GB RAM, 320 GB and 1000 GB hard drives, and a Nvidia Quadro FX 4800 graphic card, and it is running the current version of the 64-bit Arch Linux.

Preparation of Bank of Compounds. For our study, the U.S. National Cancer Institute (NCI)²⁴ bank of 280,000 compounds was selected. Because of the size of this bank, a filtering procedure was applied to provide a more focused library of compounds. To determine the optimal chemical properties that compounds need for inhibition of 3HNR, we analyzed the ligands that are known to bind to 3HNR: diclofenac, etodolac, nabumetone, phtalide, pyroquilon, tricyclazole, trihydroxynaphtalene, vermeline, and compounds **9**, **12**, and **13** from our previously published study.²⁰ All of these ligands have molecular weights between 140 g/mol and 340 g/mol, a logP between -3 and 5, a number of H-bond donors between 0 and 3, and a number of H-bond acceptors between 0 and 4. This filtering of the NCI Bank of Compounds was carried out with the filter program (Openeye Scientific Software, Inc.) and the choice of descriptors was based loosely on these properties determined for the known ligands of 3HNR: molecular weight, 120–340 g/mol; number of ring systems, 1–5; number of H-bond donors, 0–5; number of H-bond acceptors, 0–8; and logP, -5.0 to 5.0. Additional filters were used to eliminate insoluble compounds (set to moderate), to eliminate all of the compounds with atoms other than H, C, N, O, F, S, Cl, and Br, and to eliminate all of the compounds with reactive functional groups. Also, a function developed by Shoichet was implemented in the filter program, which eliminates known aggregators and which also removes the predicted aggregators.²⁵ Using this function, we anticipated the elimination of potential promiscuous inhibitors. The result from this filtering was a new subset of compounds containing roughly 72,000 structures.

3D Similarity Search. To further reduce and enrich the bank of compounds, we performed 3D similarity searches using ROCS (Openeye Scientific Software, Inc.).²⁶ The 1,3,8-trihydroxynaphtalene, substrate for 3HNR was used as a query, and the previously filtered NCI bank of compounds was used as the database. The results here were ranked according to “combo” score, which considers similarities in the molecular shape and color (atom types). In this way we obtained a new bank of 5,000 compounds that have similar shape and color to 1,3,8-trihydroxynaphtalene.

Docking. For docking experiments, FlexX 3.1 (BiosolveIT GmbH)²⁷ was used on our previously reported homology-built model of 3HNR from *C. lunata*.²⁰ To better understand the interactions needed to inhibit 3HNR, the known ligands of this enzyme were overlaid using ROCS, and a pharmacophore model was built using the Liquid plug-in²⁸ for PyMOL.²⁹ Several interaction points within the active site were identified: H-bonds with Ser149, Tyr163, Met200, and Tyr201; and π -stacking with Tyr208. For the docking, the active site was defined as the volume of the enzyme within 5.5 Å of the 4-nitro-inden-1-one ligand of the homology-built model (http://www2.mf.uni-lj.si/~stojan/THNR_NID.PDB). The cofactor NADPH was removed from the model, and essential and optional interactions were defined according to these previously identified interaction points. Not all interaction points were used, and the docking was set up in such a way that it only considered solutions that predicted π -stacking with Tyr208, and as an optional interaction, an H-bond with Ser149. For the base placement, triangle

matching was used: this program generated the maxima of 200 solutions per iteration and 200 per fragmentation.

All of the 5,000 compounds from the 3D similarity search were docked into the active site of 3HNR and ranked according to the score of the best scored conformation. From the compounds with the best scores, 19 of those available were obtained and evaluated in vitro.

Second Similarity Searching. After obtaining initial in vitro results, another 3D similarity search was performed to further explore the chemical space around the artificial substrate 2,3-dihydro-2,5-dihydroxy-4H-benzopyran-4-one (DDBO), and also around the most active of the compounds, compound **17**. This time, the complete ZINC³⁰ “drug-like” bank of 11.3 million compounds was used. A bank of compounds was prepared with Omega2 (Openeye Scientific Software, Inc.) to provide an average of 152 conformations per compound. For the 3D similarity search, ROCS was used with DDBO and compound **17** as the queries. In both cases, the hits were ranked according to “combo” score, which, as indicated above, considers the molecular shape and color similarities. Twenty-eight compounds were obtained that were available from different suppliers, of which 16 were the result of the similarity search with DDBO, and 12 of the similarity search with compound **17**.

Expression and Purification of Recombinant 3HNR. 3HNR from *C. lunata* was prepared as a glutathione S-transferase (GST)-fusion protein in *Escherichia coli* JM107 cells. This was then purified by affinity binding to glutathione–Sephacrose, followed by cleavage with thrombin, as described previously.³¹ Protein Concentrations were determined according to Bradford,³² with bovine serum albumin as the standard. The purity of the proteins was checked by SDS-PAGE on 12% polyacrilamide gels, with Coomassie blue staining.³³

Inhibition Assays. Oxidation of the nonphysiological substrate DDBO (synthesized as described previously)³⁰ to 4,5-dihydroxy-2H-benzopyran-2-one with the concomitant reduction of NADP⁺ to NADPH in the absence and presence of the tested compounds was followed using a Perkin-Elmer, Lambda 45, UV–VIS spectrophotometer. The differences in NADPH absorbance were measured at 340 nm and 25 °C. The assays were carried out in 0.8 mL 100 mM phosphate buffer, pH 8.0, with 1% dimethyl sulfoxide and 0.005% Triton X-114. The substrate concentration of 50 μ M was used, with 200 μ M coenzyme and 50 nM enzyme. The concentrations of the tested compounds were 50 μ M for screening, and 0.25–100 μ M for IC₅₀ determinations. The measurements in the screening were performed in two independent experiments, and the data are given as the means of five measurements \pm standard deviation. The measurements for the IC₅₀ value determinations were performed in triplicate. The data were analyzed as described previously,²⁰ using the GraphPad Prism version 4.00 software (GraphPad Software, Inc.).

Inhibition Mechanism. For compounds **17** and **44**, we investigated the mechanism of enzyme inhibition. These assays were carried out in 0.8 mL 100 mM phosphate buffer, pH 8.0, containing 1% dimethyl sulfoxide and 0.005% Triton X-114, as above, with 400 μ M and 800 μ M coenzyme and 60 nM and 50 nM enzyme, for compounds **17** and **44**, respectively. The concentrations of substrate were 25–450 μ M, and the concentrations of inhibitors were in the range of 0.5-fold to 2-fold of their IC₅₀. The measurements were performed in triplicates. The K_i values were calculated using the Sigma Plot 8.0 software, assisted by the Enzyme Kinetics 1.1 Module, where the initial velocity data were fitted to competitive, noncompetitive, and

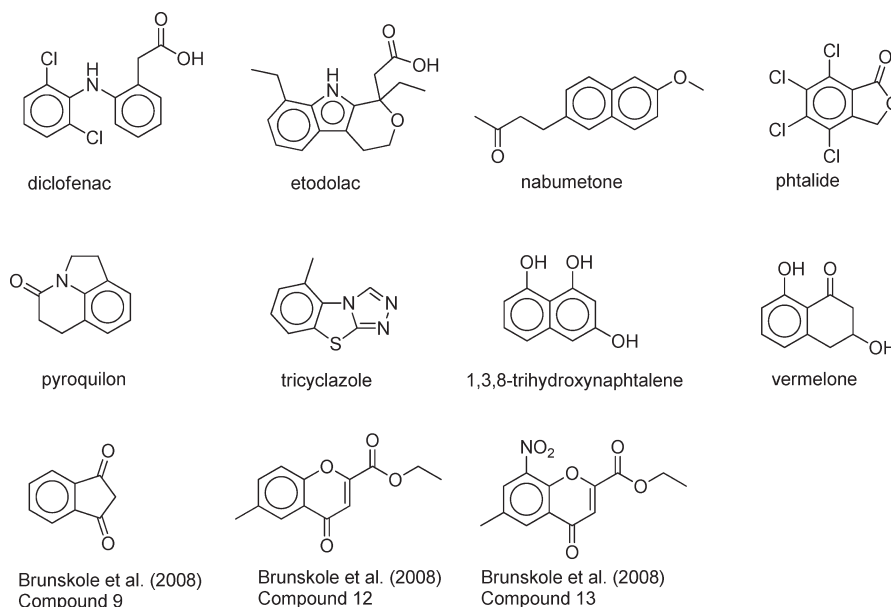


Figure 1. Ligands known to bind to the 3HNR active site.

uncompetitive inhibition models. The data show the best fit as judged by the R^2 values.

Antifungal Activity Test. The antifungal activities of four of the different compounds were tested: tricyclazole, 17, 44, and 46. Solid malt-extract agar, pH 6.5, was prepared without inhibitors (control) and with 0.5 mM of the tested compounds. Petri dishes (3.5 cm) were centrally inoculated in triplicates with 5 mm mycelia disks taken from 96 h agar culture of the fungus *C. lunata*. The inoculated plates were then incubated at 30 °C, and the growth and color of the inoculated mycelia were followed over the following week.

Compound Characterization. For compounds 1, 17, 31, 44, and 46, their purity was determined using reversed-phase high-performance liquid chromatography (HPLC) analyses performed on an Agilent 1100 system (Agilent Technologies, Santa Clara, CA, USA) equipped with a quaternary pump and a multiple-wavelength detector, using an Agilent Eclipse Plus C18, 5 μ m (150 mm \times 4.6 mm) column. The compounds were dissolved in 40% acetonitrile/water at 0.16 mg/mL final concentration, and 10 μ L was injected onto the column. Acetonitrile was used as an organic modifier and 0.1% trifluoroacetic acid in water as an aqueous buffer. The elution was performed with a 1.0 mL/min flow rate using a linear gradient from 30% to 70% acetonitrile over 15 min, followed by 2.5 min at 70% acetonitrile, then back down to 30% acetonitrile over 30 s, followed by 7 min equilibration between samples. Detection was at 220 nm. The relative purity of all of the tested compounds (except compound 1) was above 95.0%.

^1H NMR spectra were recorded on a Bruker AVANCE III 400 MHz spectrometer in DMSO- d_6 solution, with tetramethylsilane as the internal standard. Mass spectra were obtained using a VG-Analytical Autospec Q mass spectrometer.

Compound 1: HPLC purity 64.87%.

Compound 17: ^1H NMR (400 MHz, DMSO): δ 6.13 (s, 2H, $-\text{O}-\text{CH}_2-\text{O}-$); 6.92 (t, $J = 8$ Hz, 1H, Ar- $\underline{\text{H}}$); 7.07–7.09 (m, 1H, Ar- $\underline{\text{H}}$); 7.24–7.27 (m, 1H, Ar- $\underline{\text{H}}$); HPLC purity 100%; retention time = 2.74 min; HRMS (ESI) calculated for $\text{C}_8\text{H}_7\text{NO}_3$ 166.0504 $[\text{MH}]^+$, found 166.0498.

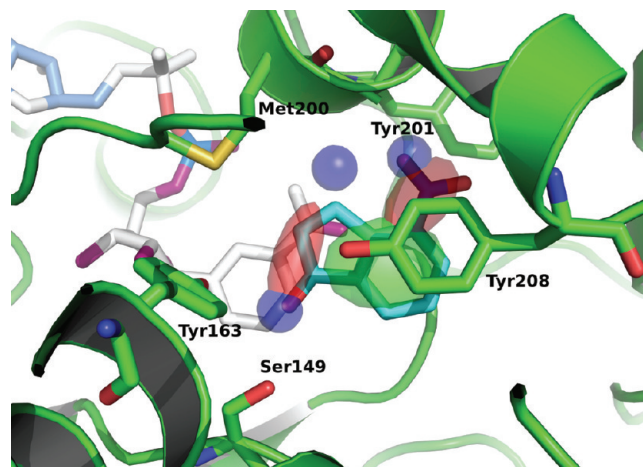


Figure 2. Active site of 3HNR from *C. lunata* with pharmacophore points arising from the known ligands. For clarity, only 4-nitro-inden-1-one (cyan) is shown. Amino-acid residues important for interactions with ligands are shown as green sticks. The cofactor NADPH (white sticks) is also shown.

Compound 31: ^1H NMR (400 MHz, DMSO): δ 2.37 (s, 3H, Ar- $\underline{\text{CH}_3}$); 2.64 (s, 3H, Ar- $\underline{\text{CH}_3}$); 2.69 (s, 3H, Ar- $\underline{\text{CH}_3}$); 6.36 (s, 1H, Ar- $\underline{\text{H}}$); 6.88 (d, $J = 7.5$ Hz, 1H, Ar- $\underline{\text{H}}$); 7.19 (d, $J = 7.3$ Hz, 1H, Ar- $\underline{\text{H}}$); HPLC purity 100%; retention time = 6.78 min; HRMS (ESI) calculated for $\text{C}_{12}\text{H}_{13}\text{NO}$ 188.1075 $[\text{MH}]^+$, found 188.1071.

Compound 44: ^1H NMR (400 MHz, DMSO): δ 7.93–7.97 (m, 1H, Ar- $\underline{\text{H}}$); 8.58–8.60 (m, 1H, Ar- $\underline{\text{H}}$); 8.68–8.70 (m, 1H, Ar- $\underline{\text{H}}$); HPLC purity 99.6%; retention time = 7.20 min; HRMS (ESI) calculated for $\text{C}_6\text{H}_3\text{N}_3\text{O}_2\text{S}$ 182.0024 $[\text{MH}]^+$, found 182.0033.

Compound 46: ^1H NMR (400 MHz, DMSO): δ 3.26 (t, $J = 8.8$ Hz, 2H, Ar- $\underline{\text{CH}_2}-\text{CH}_2-$); 4.72 (t, $J = 8.8$ Hz, 2H, $-\text{CH}_2-\underline{\text{CH}_2}-\text{O}-$); 7.58 (s, 1H, Ar- $\underline{\text{H}}$); 7.67 (s, 1H, Ar- $\underline{\text{H}}$); HPLC purity 100%; retention time = 6.36 min; HRMS (ESI) calculated for $\text{C}_9\text{H}_8\text{NO}_2\text{Br}$ 241.9817 $[\text{MH}]^+$, found 241.9818.

Table 1. Percent of Inhibition ($\% \pm \text{SD}^*$) of the Compounds Evaluated Biochemically after the Virtual Screening (listed with supplier and supplier code)

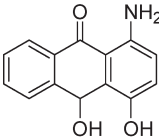
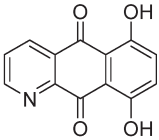
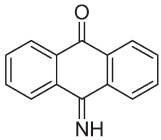
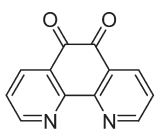
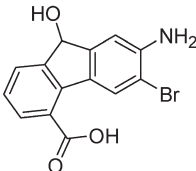
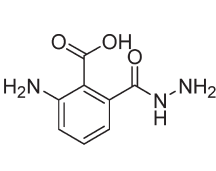
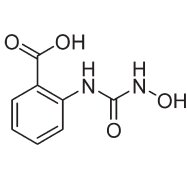
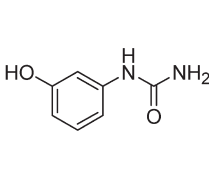
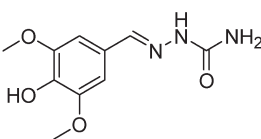
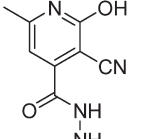
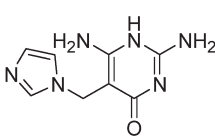
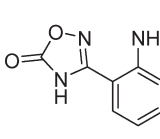
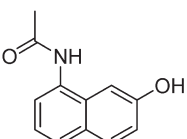
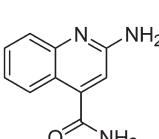
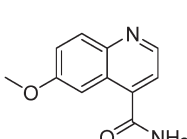
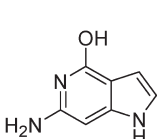
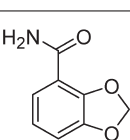
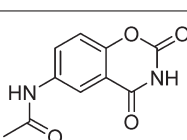
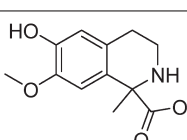
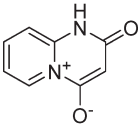
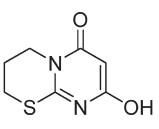
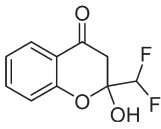
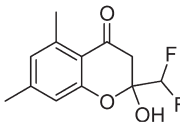
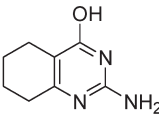
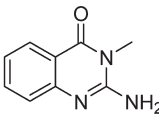
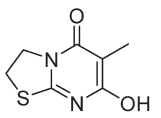
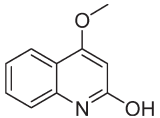
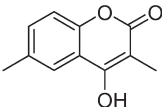
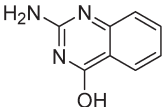
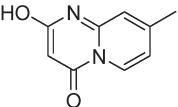
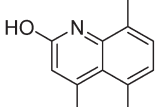
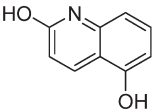
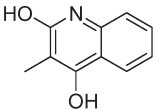
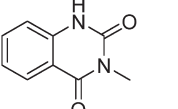
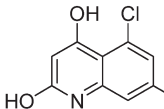
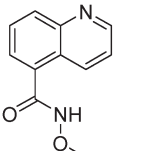
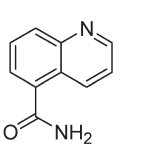
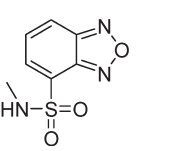
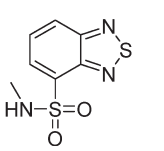
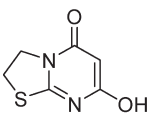
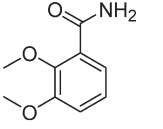
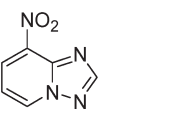
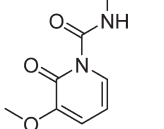
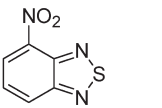
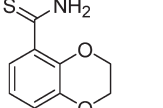
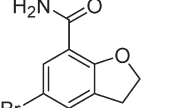
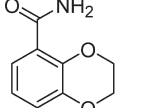
Compounds selected after initial virtual screening			
 1 $60 \pm 2.8\%$ NCI 401148	 2 $38 \pm 5.6\%$ NCI 101510	 3 $23 \pm 9.5\%$ NCI 135187	 4 $34 \pm 5.2\%$ NCI 346882
 5 $5.6 \pm 9.1\%$ NCI 121309	 6 $3.6 \pm 7.4\%$ NCI 60142	 7 $9.0 \pm 6.0\%$ NCI 92754	 8 $9.5 \pm 9.4\%$ NCI 60733
 9 $3.0 \pm 10.4\%$ NCI 318210	 10 insoluble NCI 18347	 11 insoluble NCI 87450	 12 $0 \pm 5.9\%$ NCI 686354
 13 $9.8 \pm 2.9\%$ NCI 7566	 14 $7.2 \pm 4.9\%$ NCI 26049	 15 $8.6 \pm 3.7\%$ NCI 27532	 16 $9.0 \pm 2.8\%$ NCI 328159
 17 $88 \pm 2.4\%$ NCI 146453	 18 $-3.3 \pm 7.6\%$ NCI 50119	 19 insoluble NCI 267397	
Compounds selected after second virtual screening			
Compounds from 3D similarity to DDBO			
 20 $4.6 \pm 2.2\%$ ChemBridge 5517757	 21 $1.4 \pm 5.3\%$ ChemBridge 5240510	 22 $-0.8 \pm 5.8\%$ ChemBridge 5483149	 23 $20.3 \pm 3.2\%$ ChemBridge 6886732
 24 $1.8 \pm 3.5\%$ Apollo Scientific OR8486	 25 $1.0 \pm 4.0\%$ InterBioScreen 98325 STOCK2S-	 26 $-0.8 \pm 4.9\%$ Specs AE-406/41056843	 27 $2.0 \pm 5.0\%$ Specs AE-562/12222666

Table 1. Continued

Compounds selected after second virtual screening			
Compounds from 3D similarity to DDBO			
 28 3.4 ±6.3% TimTec ST5308839	 29 -0.7 ±2.0% NCI 51782	 30 0.2 ±4.5% NCI 102020	 31 61.9 ±2.0% NCI 109754
 32 6.2 ±3.4% NCI 134652	 33 0.9 ±6.4% NCI 193538	 34 3.5 ±6.6% NCI 401253	 35 2.1 ±3.3% Maybridge RH01004SC
Compounds from 3D similarity to compound 17			
 36 -1.2 ±4.3% Enamine T6108076	 37 0.9 ±4.8% Enamine T6205275	 38 8.3 ±2.3% Vitas-M STK461264	 39 33.3 ±6.1% InterBioScreen STOCK3S-06956
 40 4.5 ±4.4% InterBioScreen STOCK1S-86808	 41 5.3 ±4.4% NCI 40843	 42 1.4 ±6.2% NCI 116466	 43 5.2 ±4.4% NCI 281257
 44 >90% NCI 404747	 45 -0.3 ±6.2% Maybridge CC01418CB	 46 >90% Maybridge KM07182SC	 47 32.3 ±4.3% Maybridge MO00789SC

* Percent of inhibition represents mean of 5 measurements at 50 μ M compound \pm standard deviation.

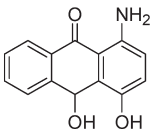
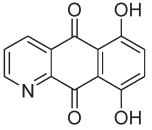
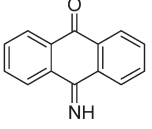
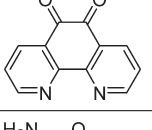
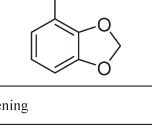
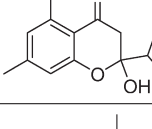
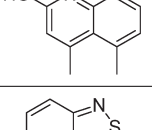
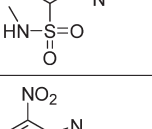
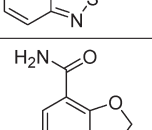
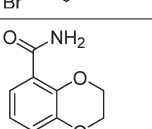
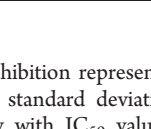
RESULTS AND DISCUSSION

Initial Virtual Screening. Preparation of Bank of Compounds, Filtering and Ligand-Based 3D Similarity Searching. For the initial virtual screening, the U.S. National Cancer Institute (NCI) bank of 280,000 compounds was selected. Because of the size of this bank and also because it contains compounds with unwanted properties, an initial filtering procedure based on simple molecular descriptors was applied first. These descriptors were selected by analysis of the known inhibitors of 3HNR (Figure 1).

To further enrich the bank of compounds, a ligand-based 3D similarity search was implemented in ROCS (OpenEye Scientific

Software, Inc.).²⁶ ROCS overlays the chemical structures with the query structure and then compares their shapes and the chemical types of their atoms (expressed as color) and ranks the compounds according to their similarities, which provides a score according to this combination of shape and color.²⁶ A 3D similarity method was chosen because these types of methods tend to give chemically more diverse hits compared to those of classical 2D methods.^{34,35} The physiological substrate of 3HNR, 1,3,8-trihydroxynaphthalene, was used as the query for the ligand-based 3D similarity search, with the previously filtered NCI bank of compounds as the database. In all, the top 5000 compounds, according to the best shape and color scores, were kept for the docking experiments.

Table 2. Biochemically Identified Inhibitors of 3HNR

Compound	Structure	Inhibition (%) \pm SD*	IC ₅₀ (μ M) (Hill coefficient)**
Initial virtual screening			
1		60 \pm 2.8	14.5 (0.62)
2		38 \pm 5.6	
3		23 \pm 9.5	
4		34 \pm 5.2	
17		88 \pm 2.4	8.2 (0.99)
Second virtual screening			
23		20.3 \pm 3.2	
31		61.9 \pm 2.0	29 (0.90)
39		33.4 \pm 6.1	
44		> 90	0.82 (0.94)
46		>90	1.9 (1.05)
47		32.3 \pm 4.3	

* Percent of inhibition represents mean of 5 measurements at 50 μ M compound \pm standard deviation. ** Hill coefficient was determined simultaneously with IC₅₀ values, to eliminate promiscuous binders, according to Shoichet.²⁵

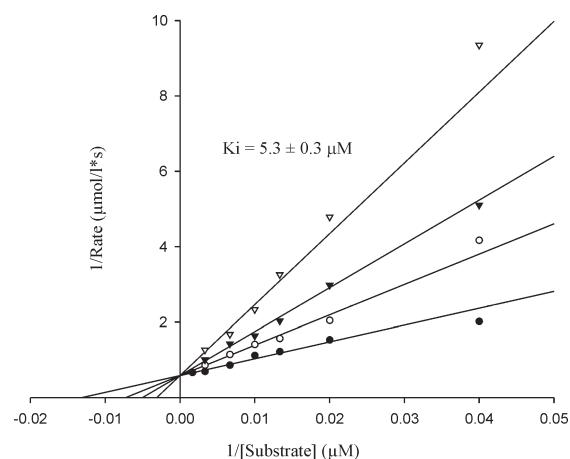


Figure 3. Kinetics analysis of inhibition of 3HNR by compound 17. Lineweaver–Burk plot of the reciprocal of the initial velocity versus the reciprocal concentrations of DDBO at different fixed concentrations of compound 17: 0 μ M (●), 4 μ M (○), 8 μ M (□), and 16 μ M (▽). Measurements were performed at saturating NADP⁺ concentrations of 400 μ M.

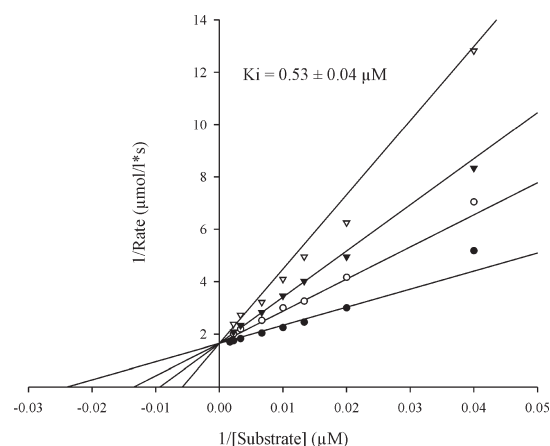


Figure 4. Kinetics analysis of inhibition of 3HNR by compound 44. Lineweaver–Burk plot of the reciprocal of the initial velocity versus the reciprocal concentrations of DDBO at different fixed concentrations of compound 44: 0 μ M (●), 0.4 μ M (○), 0.8 μ M (□), and 1.6 μ M (▽). Measurements were performed at saturating NADP⁺ concentrations of 800 μ M.

Molecular Docking. As the crystal structure of 3HNR from *C. lunata* is not known, our previously reported homology-built model was used for the molecular docking.²⁰ It needs to be stressed here that the model was worked out using 3HNR from *Magnaporthe grisea*³⁶ and the 17 β -HSDc1³⁷ crystal structures as templates. The 74% and 58% sequence identities obtained for 3HNR of *M. grisea* and 17 β -HSDc1, respectively, allowed us to assume that the model would be within 1 Å rms of the reality. Moreover, the residues lining the active site of 3HNR from *C. lunata* are all identical with their counterparts in 3HNR from *M. grisea*. To better understand possible interaction points with the active site and to facilitate the design of the docking experiment, the previously mentioned ligands (diclofenac, etodolac, nabumetone, phtalide, pyroquilon, tricyclazole, trihydroxynaphthalene, vermeline, and compounds 9, 12, and 13 from our

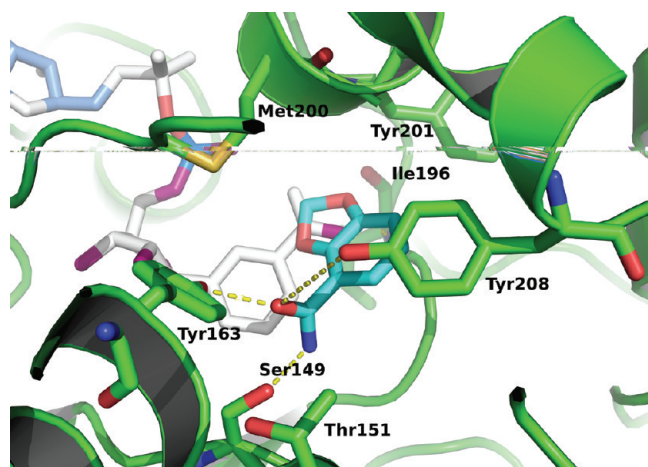


Figure 5. Compound 17 (cyan) docked into the active site of 3HNR. The H-bonds with Ser149, Tyr163, Ile196, and Tyr208 are shown as yellow dashes.

previously published study²⁰) were overlaid using ROCS, on 4-nitro-inden-1-one, a ligand for which the position has been solved for 3HNR from *M. grisea* and which was originally docked in the homology-built model of 3HNR from *C. lunata*. Using a Liquid plugin²⁸ for PyMOL,²⁹ a pharmacophore model was built. Several interaction points within the active site were identified: H-bonds with Ser149, Tyr163, Met200, and Tyr201; and π -stacking with Tyr208 (Figure 2).

The docking experiments were carried out with FlexX 3.1 (BiosolveIT GmbH).²⁷ For these docking experiments, the active site was defined as the volume of the enzyme within 5.5 Å around the ligand from the homology-built model. The cofactor NADPH was removed from the model. The docking experiments were set up in such a way that only solutions predicting π -stacking with Tyr208 were considered, with an optional interaction of H-bonding with Ser149. All of the 5000 compounds from the ligand-based 3D similarity search were docked into this active site and ranked according to the score predicted by FlexX. From the highest ranked compounds, 19 that were available were selected and obtained from NCI (Table 1).

Biochemical Evaluation of Initial Hits. Out of the 19 compounds obtained, compounds 10, 11, and 19 were insoluble. For the other 17 compounds, the percentage of inhibition of 3HNR at 50 μ M of each compound was determined. Compounds with percentage of inhibition higher than 20 were considered as inhibitors. Among these, compounds with percentage of inhibition between 20 and 60 (compounds 2, 3, and 4) were considered as modest binders and compounds with percentage of inhibition higher than 60 (compounds 1 and 17) were considered as potent binders (Table 2). Structurally, compounds 1, 2, 3, and 4 are three-ring-containing compounds with anthracene (1 and 3), benzoquinoline (2), and 1,10-phenanthroline (4) scaffolds. Compound 17 is a benzo-1,3-dioxole derivative.

For compounds 1 and 17, IC₅₀ values of 14.5 and 8.2 μ M, respectively, were obtained. As the purity of compound 1 was only 64.7%, it was not evaluated further. Compound 17 was the best inhibitor in this series, and the further kinetics analysis revealed that it is a competitive inhibitor with a determined K_i value of 5.3 ± 0.3 μ M (Figure 3). The competitive mode of inhibition is in agreement with our expectations, as the tested compounds were selected on the basis of their docking simulation in the enzyme active site.

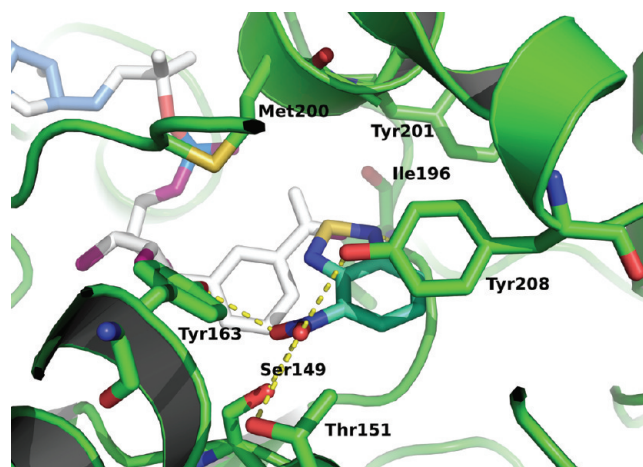


Figure 6. Compound 44 (cyan) docked into the active site of 3HNR. The H-bonds with Ser149, Thr151, Tyr163, Ile196, and Tyr208 are shown as yellow dashes.

Second Virtual Screening and Biochemical Evaluation. Given the promising in vitro results, we decided to follow another ligand-based 3D similarity search for compounds similar to the artificial substrate DDBO and compound 17. This time, a larger bank of 11.3 million ZINC “drug-like” compounds was used. Prior to the 3D similarity search, the bank of compounds was prepared with Omega2 (OpenEye Scientific Software Inc.) to yield an average 152 conformations per compound. ROCS was then used to screen this bank for compounds similar in shape and color to DDBO and compound 17. Twenty-eight of the available compounds were obtained from different suppliers, of which 16 were the result of similarity to DDBO and 12 to compound 17 (Table 1).

All of these 28 compounds were assayed for inhibition of 3HNR. Those that showed inhibition of 3HNR were chroman-4-one (23), quinoline (31), benzo-1,2,5-thiadiazole (39 and 44), 2,3-dihydrobenzofuran (46), and 2,3-dihydrobenzo-1,4-dioxine (47) derivatives. Compounds with percentage of inhibition higher than 20 were considered as inhibitors. Among these, compounds with percentage of inhibition between 20 and 60 (compounds 23, 39, and 47) were considered as modest binders and compounds with percentage of inhibition higher than 60 (compounds 31, 44, and 46) were considered as potent binders (Table 2). Compounds 31, 44, and 46 have IC₅₀ values of 29, 0.82, and 1.9 μ M, respectively. Compound 31 originated from the 3D similarity search for DDBO analogues and compounds 44 and 46 from the 3D similarity search for compound 17 analogues. The kinetics studies revealed that compound 44 is a competitive inhibitor of 3HNR with a K_i value of 0.53 ± 0.04 μ M (Figure 4).

Docking of Compounds 17 and 44 into the Active Site of 3HNR. As has been shown in the literature, ligand-based methods can give good results, and interestingly, docking to homology-built models appears to give better results than docking to crystal structures.³⁸ The method of virtual screening used in the present study was based on the combination of ligand-based 3D similarity searching and structure-based docking to the homology-built model of 3HNR. According to our docking study, compound 17 binds within the active site by forming H-bonds with the OH groups of Ser149, Tyr163, Tyr208, and with the backbone NH of Ile196, and π -stacking interactions with Tyr201 and Tyr208 (Figure 5).

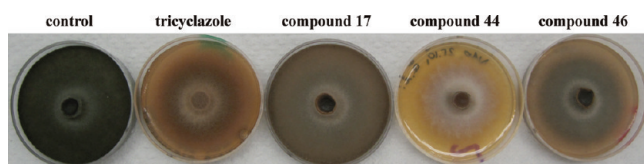


Figure 7. Inhibition of *C. lunata* cultures on malt-extract media by tricyclazole and compounds 17, 44, and 46 (all at 0.5 mM). After 71 h growth, the control cultures were dark-gray to black, while the inhibited cultures were tricyclazole, reddish-brown; compound 17, light-brown to light-gray; compound 44, white; and compound 46, dark brown.

To better understand the binding mode of compound 44, the same docking procedure was used as before. According to our docking study, compound 44 binds within the active site by forming H-bonds with the OH groups of Ser149, Thr151, Tyr163, Tyr208, and with the backbone NH of Ile196, and π -stacking interactions with Tyr208 (Figure 6). Compound 44 forms one H-bond more within the active site compared to compound 17, which is in agreement with the better inhibitory activity of compound 44.

Antifungal Activity. The antifungal activities of compounds 17, 44, and 46, and with tricyclazole as the positive control, were tested (all at 0.5 mM). *C. lunata* was grown on malt-extract agar in the absence and presence of the tested compounds, and the pigmentation and growth of the *C. lunata* were followed over the next few days. After 71 h growth, the control colony (with no inhibitor) was dark-gray to black, while the tricyclazole-inhibited colony was reddish-brown, and the radius of the colony was smaller in comparison to the control (Figure 7). Tricyclazole, a commercially available inhibitor of 3HNR from *M. grisea*, not only affected fungal pigmentation, but also affected fungal growth.

Compounds 17, 44, and 46 also affected fungal growth and pigmentation. In the presence of compound 44, the most potent inhibitor in the present study, the radii of the colonies were approximately half the radii of the control, and the colonies were almost white. Compound 17 inhibited fungal growth slightly, and the colonies were light brown to light gray. Compound 46 affected fungal growth comparable to the positive control, but the colonies were dark brown. After further days of growth, the colonies with compounds 17, 44, and 46 became darker; however, the positive control colony with tricyclazole remained reddish-brown. As already discussed,²² this can be explained by the approximately 250-fold to 2500-fold lower affinity of the inhibitors toward 3HNR as compared to tricyclazole ($K_i = 2$ nM).²³ Although the antifungal activity test is not quantitative, a correlation between the IC_{50} values of compounds 17, 44, and 46 and their effects on growth and pigmentation of *C. lunata* was observed, which suggests that the antifungal activity seen is most probably a consequence of inhibition of 3HNR.

CONCLUSIONS

A combination of ligand-based 3D similarity searching and structure-based docking to a homology-built model have been shown here to be a suitable method for searching for inhibitors of 3HNR from *C. lunata*. Nineteen compounds from the initial search and 28 compounds from the second virtual screening were evaluated biochemically, and among these, for the most potent five compounds, their IC_{50} values were determined. Hit compound 17 from the initial search inhibits 3HNR in a competitive manner with a K_i of 5.3 ± 0.3 μ M. In subsequent ligand-based 3D

similarity searches based on compounds with a similar molecular shape and color as compound 17, compound 44 was identified with 10-fold greater activity ($K_i = 0.53 \pm 0.04$ μ M) in comparison to compound 17. With the discovery of inhibitor 31 (IC_{50} , 29 μ M), we have also demonstrated that a substrate (DDBO) can be successfully used as a query for ligand-based 3D similarity searches. It is also worth noting that our approach gave high hit rates with 5 out of 19 (26.3%) hits from 3D similarity search with subsequent docking experiment and 2 out of 16 (12.5%) and 4 out of 12 (33.3%) of hits for 3D similarity search for compounds with a similar molecular shape and color to the DDBO and compound 17, respectively. Compounds 17, 44, and 46 also affect fungal growth and pigmentation, and these are therefore promising lead compounds for the development of future fungicides and antimycotics.

AUTHOR INFORMATION

Corresponding Author

* Tel: +386-1-4769500. Fax: +386-1-4258031. E-mail: Stanislav.Gobec@ffa.uni-lj.si.

ACKNOWLEDGMENT

This work was supported by an ARRS Grant and 2011 L'OREAL - UNESCO fellowship "For Women in Science", both awarded to M.B.Š. as a young researcher. We thank OpenEye Scientific Software, Inc. for free academic licenses of their software, and the Drug Synthesis and Chemistry Branch, Developmental Therapeutics Program, Division of Cancer Treatment and Diagnosis, National Cancer Institute, for supplying the compounds for testing. We also thank Dr. Joško Cesar for HPLC analyses and Dr. Chris Berrie for critical reading of the manuscript.

REFERENCES

- (1) Rinaldi, M. G.; Phillips, P.; Schwartz, J. G.; Winn, R. E.; Holt, G. R.; Shagets, F. W.; Elrod, J.; Nishioka, G.; Aufdemorte, T. B. Human *Curvularia* infections. Report of five cases and review of the literature. *Diagn. Microbiol. Infect. Dis.* **1987**, *6*, 27–39.
- (2) Prom, L. K.; Waniska, R. D.; Kollo, A. I.; Rooney, W. L. Response of eight sorghum cultivars inoculated with *Fusarium thapsinum*, *Curvularia lunata*, and a mixture of the two fungi. *Crop Prot.* **2003**, *22*, 623–628.
- (3) Masratul Hawa, M.; Salleh, B.; Latiffah, Z. First report of *Curvularia lunata* on red-fleshed dragon fruit (*Hylocereus polyrhizus*) in Malaysia. *Plant Dis.* **2009**, *93*, 971.
- (4) Bartynski, J. M.; McCaffrey, T. V.; Frigas, E. Allergic fungal sinusitis secondary to dermatiaceous fungi: *Curvularia lunata* and *Alternaria*. *Otolaryngol.—Head Neck Surg.* **1990**, *103*, 32–39.
- (5) Bryan, C. S.; Smith, C. W.; Berg, D. E.; Karp, R. B. *Curvularia lunata* endocarditis treated with terbinafine: Case report. *Clin. Infect. Dis.* **1993**, *16*, 30–32.
- (6) Lopes, J. O.; Alves, S. H.; Benevenga, J. P.; Brauner, F. B.; Castro, M. S.; Melchior, E. *Curvularia lunata* peritonitis complicating peritoneal dialysis. *Mycopathologia* **1994**, *127*, 65–67.
- (7) Janaki, C.; Sentamilselvi, G.; Janaki, V. R.; Devesh, S.; Ajithadas, K. Case report. Eumycetoma due to *Curvularia lunata*. *Mycoses* **1999**, *42*, 345–346.
- (8) Garg, A.; Sujatha, S.; Garg, J.; Parija, S. C.; Thappa, D. M. Eumycetoma due to *Curvularia lunata*. *Indian J. Dermatol. Venereol. Leprol.* **2008**, *74*, S15–S16.
- (9) Wilhelmus, K. R.; Jones, D. B. *Curvularia* keratitis. *Trans. Am. Ophthalmol. Soc.* **2001**, *99*, 111–130.
- (10) Travis, W. D.; Kwon-Chung, K. J.; Kleiner, D. E.; Geber, A.; Lawson, W.; Pass, H. I.; Henderson, D. Unusual aspects of allergic

bronchopulmonary fungal disease: report of two cases due to *Curvularia* organisms associated with allergic fungal sinusitis. *Hum. Pathol.* **1991**, *22*, 1240–1248.

(11) Kaushik, S.; Ram, J.; Chakrabarty, A.; Dogra, M. R.; Brar, G. S.; Gupta, A. *Curvularia lunata* endophthalmitis with secondary keratitis. *Am. J. Ophthalmol.* **2001**, *131*, 140–142.

(12) Smith, T.; Goldschlager, T.; Mott, N.; Robertson, T.; Campbell, S. Optic atrophy due to *Curvularia lunata* mucocoele. *Pituitary* **2007**, *10*, 295–297.

(13) Revankar, S. G.; Patterson, J. E.; Sutton, D. A.; Pullen, R.; Rinaldi, M. G. Disseminated phaeohyphomycosis: Review of an emerging mycosis. *Clin. Infect. Dis.* **2002**, *34*, 467–476.

(14) Carter, E.; Boudreaux, C. Fatal cerebral phaeohyphomycosis due to *Curvularia lunata* in an immunocompetent patient. *J. Clin. Microbiol.* **2004**, *42*, 5419–5423.

(15) Polak, A. Melanin as a virulence factor in pathogenic fungi. *Mycoses* **1990**, *33*, 215–224.

(16) Nosanchuk, J. D.; Casadevall, A. The contribution of melanin to microbial pathogenesis. *Cell. Microbiol.* **2003**, *5*, 203–223.

(17) Plonka, P. M.; Grabacka, M. Melanin synthesis in microorganisms: Biotechnological and medical aspects. *Acta Biochim. Pol.* **2006**, *53*, 429–443.

(18) Bell, A. A.; Wheeler, M. H. Biosynthesis and functions of fungal melanins. *Ann. Rev. Phytopathol.* **1986**, *411–451*.

(19) Abdel-Fattah, A. F.; Ismail, A. M. Preparation and properties of fibrinolytic enzymes produced by *Cochliobolus lunatus*. *Biotechnol. Bioeng.* **1984**, *26*, 37–40.

(20) Brunskole, M.; Štefane, B.; Zorko, K.; Anderluh, M.; Stojan, J.; Lanišnik Rižner, T.; Gobec, S. Towards the first inhibitors of trihydroxynaphthalene reductase from *Curvularia lunata*: Synthesis of artificial substrate, homology modelling and initial screening. *Bioorg. Med. Chem.* **2008**, *16*, 5881–5889.

(21) Lanišnik Rižner, T.; Wheeler, M. H. Melanin biosynthesis in the fungus *Curvularia lunata* (teleomorph: *Cochliobolus lunatus*). *Can. J. Microbiol.* **2003**, *49*, 110–119.

(22) Brunskole, M.; Zorko, K.; Kerbler, V.; Martens, S.; Stojan, J.; Gobec, S.; Lanišnik Rižner, T. Trihydroxynaphthalene reductase of *Curvularia lunata*: A target for flavonoid action? *Chem Biol. Interact.* **2009**, *178*, 259–267.

(23) Jordan, D. B.; Basarab, G. S.; Liao, D. I.; Johnson, W. M.; Winzenberg, K. N.; Winkler, D. A. Structure-based design of inhibitors of the rice blast fungal enzyme trihydroxynaphthalene reductase. *J. Mol. Graph. Model* **2001**, *19* (434–447), 470–431.

(24) NCI DTP Discovery Services. <http://www.dtp.nci.nih.gov> (accessed March 23, 2011).

(25) Shoichet, B. K. Interpreting steep dose–response curves in early inhibitor discovery. *J. Med. Chem.* **2006**, *49*, 7274–7277.

(26) Grant, J. A.; Gallardo, M. A.; Pickup, B. T. A fast method of molecular shape comparison: A simple application of a Gaussian description of molecular shape. *J. Comput. Chem.* **1996**, *17*, 1653–1666.

(27) Rarey, M.; Kramer, B.; Lengauer, T.; Klebe, G. A fast flexible docking method using an incremental construction algorithm. *J. Mol. Biol.* **1996**, *261*, 470–489.

(28) Tanrikulu, Y.; Nietert, M.; Scheffer, U.; Proschak, E.; Grabowski, K.; Schneider, P.; Weidlich, M.; Karas, M.; Gobel, M.; Schneider, G. Scaffold hopping by “fuzzy” pharmacophores and its application to RNA targets. *ChemBioChem* **2007**, *8*, 1932–1936.

(29) The PyMOL Molecular Graphics System, version 1.3.1; Schrödinger, L. L. C.: New York, 2010.

(30) Irwin, J. J.; Shoichet, B. K. ZINC: A free database of commercially available compounds for virtual screening. *J. Chem. Inf. Model* **2005**, *45*, 177–182.

(31) Lanišnik Rižner, T.; Möller, G.; Thole, H. H.; Žakelj Mavrič, M.; Adamski, J. A novel 17 β -hydroxysteroid dehydrogenase in the fungus *Cochliobolus lunatus*: New insights into the evolution of steroid-hormone signalling. *Biochem. J.* **1999**, *337*, 425–431.

(32) Bradford, M. M. A rapid and sensitive method for the quantitation of microgram quantities of protein utilizing the principle of protein-dye binding. *Anal. Biochem.* **1976**, *72*, 248–254.

(33) Laemmli, U. K. Cleavage of structural proteins during the assembly of the head of bacteriophage T4. *Nature* **1970**, *227*, 680–685.

(34) Böhm, H.-J.; Flohr, A.; Stahl, M. Scaffold hopping. *Drug Discovery Today: Technol.* **2004**, *1*, 217–224.

(35) Rush, T. S.; Grant, J. A.; Mosyak, L.; Nicholls, A. A shape-based 3-D scaffold hopping method and its application to a bacterial protein-protein interaction. *J. Med. Chem.* **2005**, *48*, 1489–1495.

(36) Andersson, A.; Jordan, D.; Schneider, G.; Lindqvist, Y. Crystal structure of the ternary complex of 1,3,8-trihydroxynaphthalene reductase from *Magnaporthe grisea* with NADPH and an active-site inhibitor. *Structure* **1996**, *4*, 1161–1170.

(37) Cassetta, A.; Büdefeld, T.; Lanišnik Rižner, T.; Kristan, K.; Stojan, J.; Lamba, D. Crystallization, X-ray diffraction analysis and phasing of 17 β -hydroxysteroid dehydrogenase from the fungus *Cochliobolus lunatus*. *Acta Crystallogr. Sect. F. Struct. Biol. Cryst. Commun.* **2005**, *61*, 1032–1034.

(38) Ripphausen, P.; Nisius, B.; Peltason, L.; Bajorath, J. Quo vadis, virtual screening? A comprehensive survey of prospective applications. *J. Med. Chem.* **2010**, *53*, 8461–8467.